Multiple echoes in beam spin-echo spectroscopy and their effect on measurements of ultra-fast dynamics

OPEN ACCESS
IOP Publishing
Journal of Physics: Condensed Matter
J. Phys.: Condens. Matter **34** (2022) 345901 (11pp)
https://doi.org/10.1088/1361-648X/ac7765

Multiple echoes in beam spin-echo spectroscopy and their effect on measurements of ultra-fast dynamics

Helen Chadwick*, Joshua T Cantin, Yosef Alkoby and Gil Alexandrowicz*

Department of Chemistry, Faculty of Science and Engineering, Swansea University, Swansea SA2 8PP, United Kingdom

E-mail: h.j.chadwick@swansea.ac.uk and g.n.alexandrowicz@swansea.ac.uk

Received 7 April 2022, revised 25 May 2022
Accepted for publication 9 June 2022
Published 22 June 2022

Abstract

Helium (^{3}He) spin-echo is a powerful experimental technique used to probe ultra-fast atomic scale surface dynamics. The analysis of these measurements is typically performed assuming there is only a single spin-echo condition, expected to produce a constant signal for pure elastic scattering, a monotonically decaying signal for quasi-elastic scattering and oscillations from inelastic scattering events. In the present work, we show that there are in fact four spin-echoes which must be correctly accounted for, and that even in the case of elastic scattering these additional echoes lead to oscillations which could mistakenly be interpreted as being due to inelastic scattering. We demonstrate that it is possible to accurately simulate the experimental data by propagating the ^{3}He through the measured magnetic field profile of the apparatus and considering the geometry of the machine, allowing the effect of these additional echoes to be disentangled from inelastic scattering events in future ^{3}He spin-echo measurements.

Keywords: helium spin-echo, atomic beams, surface scattering

(Some figures may appear in colour only in the online journal)

1. Introduction

Neutron spin-echo (NSE) and its daughter technique, helium spin-echo (HSE), revolutionised the ability to measure bulk and surface dynamics [1, 2]. Both techniques make use of a similar magnetic manipulation scheme on spin $^1/_2$ particles (neutrons or ^{3}He atoms), which circumvents the resolution limitations related to the energy spread of the beam particles, in order to detect subtle energy exchanges during the scattering event, orders of magnitude smaller than the energy spread of the incident beam.

The theoretical foundations of the experimental technique, and correspondingly the methods which should be used to interpret spin-echo measurements, have been described using various approaches. These include the original classical derivation [3], approximate quantum mechanical derivations [4], a graphical 2d Fourier transform method [5–7], in addition to others. A common aspect of all these theoretical descriptions is that they result in a single condition for the magnetic fields where the spin phase of particles with different velocities contribute constructively to the signal, termed the spin-echo condition. Crudely speaking, this spin-echo condition represents the case where the velocity dependent spin phase, encoded by an electromagnet before the particles scatter from the sample, is cancelled by applying a second magnetic field

* Authors to whom any correspondence should be addressed.

after the scattering event which reverses the phase, and any loss of coherency is related to energy changes during the scattering process. This is a beam experiment analogue to the original Hahn spin-echo sequence measured routinely in NMR experiments [8].

Whilst theoretical explanations of beam spin-echo experiments (NSE and HSE) mentioned above were successfully used to design, execute and interpret a wide range of measurements over the years, they all miss other spin-echo conditions as the result of an over simplified treatment of the apparatus. Interestingly, the identification of a second spin-echo condition in spin $1/2$ systems [9] resulted from the necessity to develop more detailed theoretical treatments to describe molecular beam experiments which are inherently complex due to the multitude of quantum states [10–13]. In this paper, we present a further two spin-echo conditions in spin $1/2$ spin-echo experiments, which we denote as the X and X' echoes. These additional echoes are related to the magnetic beam profiles of a realistic, rather than ideal, experimental apparatus. We then show how the parallel and anti-parallel echoes [9], as well as the X and X' echoes, affect a standard spin-echo measurement. Depending on the exact experimental conditions, the additional spin-echo signals result in an oscillatory signal which could be interpreted erroneously as an inelastic excitation.

2. Experimental methods

A schematic overview of the experimental apparatus used in the current study is shown in figure 1. The atomic beam of ^{3}He is generated by expanding the gas through a nozzle held at 40 K which gives a central velocity of approximately 725 m s^{-1}, where the two nuclear spin projection states of ^{3}He ($m_I = 1/2$ and $m_I = -1/2$) are equally populated. This beam passes through a hexapole [14] where the low field seeking states ($m_I = 1/2$) are focussed and the high field seeking states ($m_I = -1/2$) defocussed, so that only the $m_I = 1/2$ state is significantly populated at the end of the hexapole meaning that only this state contributes to the signal. A dipole adiabatically rotates the spins at the end of the hexapole to lie along the z direction, which defines the quantisation axis for the propagation of the spins down the first arm of the apparatus. At this point, the wavefunction associated with the nuclear spin state can be considered as a pure state in the z frame of reference due to the strong magnetic field gradients which decohered any super-position states [15].

After a zero-field region, the atoms enter solenoid 1, an electromagnet which creates a tuneable magnetic field with integral, B_1, along the x-axis where a positive field value corresponds to a field direction which is anti-parallel with respect to the direction of propagation, and a negative field value a direction which is parallel with respect to the direction of propagation. The initially pure spin state along z, is not an eigen-state in a magnetic field along x, and the field changes both the amplitudes and the phases of the superposition wavefunction as the atom passes through the field region. This Rabi oscillation of the complex amplitudes of the quantum state can also be understood in the classical picture as Larmor precession of the magnetic moment within the yz plane. Due to the velocity spread in the molecular beam (which is approximately 60 m s^{-1} full width at half maximum in the experiments presented below) the atoms will spend different times within the field region and consequently undergo different evolutions of the wavefunction, or in the classical picture accumulate different phases within the yz plane, by the time they reach the end of the first solenoid.

The ^{3}He then passes through a set of Helmholtz coils which can be used to generate a small tuneable magnetic field along the y direction, the role of which we discuss later, before scattering from the Cu(111) surface held at a surface temperature of 300 K. As the surface is non-magnetic the m_I state is not changed by the collision. In the present work, we will focus on specular scattering conditions which ensure that the signal we observe is essentially completely due to elastic scattering.

After scattering, the atoms pass through a second solenoid with magnetic field integral, B_2, where the magnetic field is directed along the x'-axis (again positive field values are anti-parallel to the direction of the propagation of the atoms). Within the second solenoid the complex amplitudes of the superposition quantum states oscillate again, or thinking of this classically, the spins perform Larmor precession in the $y'z'$ plane. The atoms then pass through a second dipole which is directed along the $-z'$ direction which defines the quantisation axis for the propagation of the spins through the second arm of the machine. They then go through a second hexapole [16] which again focusses the low field seeking states and defocusses the high field seeking states, before reaching a highly sensitive custom built detector [17] to produce the measured signal.

The standard spin-echo condition, derived originally for neutron scattering, is that the second magnetic field integral is equal in magnitude but opposite in direction to the one produced in the first solenoid (i.e. $B_1 = -B_2$), this can be intuitively understood using the following argument; while the atoms have different velocities and complete a different amount of precessions in the first coil, the fact that the scattering is elastic (or quasi-elastic [1, 6]), means that each of them will undergo a reversed precession in the second coil, and they will all return to their original spin phase, contributing constructively to a measurable signal. Due to the simplicity of the standard echo condition, it can be realised experimentally by building two essentially identical electromagnets [18], connecting them in series, and passing the same current through both of them but with a reversed polarity for one of the two. However, due to the scattering angle, and the non-adiabatic transitions between the fields, a condition of $B_1 = B_2$ also gives rise to a parallel echo [9], in fact for instruments with a total scattering angle smaller than 90 degrees the parallel echo is the dominant signal. As we will show below, spin-echoes can also be observed for different values of B_1 and B_2, when realistic magnetic beam profiles are taken into consideration. To study these echoes, we need to be able to control the current in each electromagnet separately. In practice this is done using two independent high stability power supplies (Danfysik) which stabilise the currents with an accuracy on the order of a few ppm. A pause of 0.1 s was used to allow the

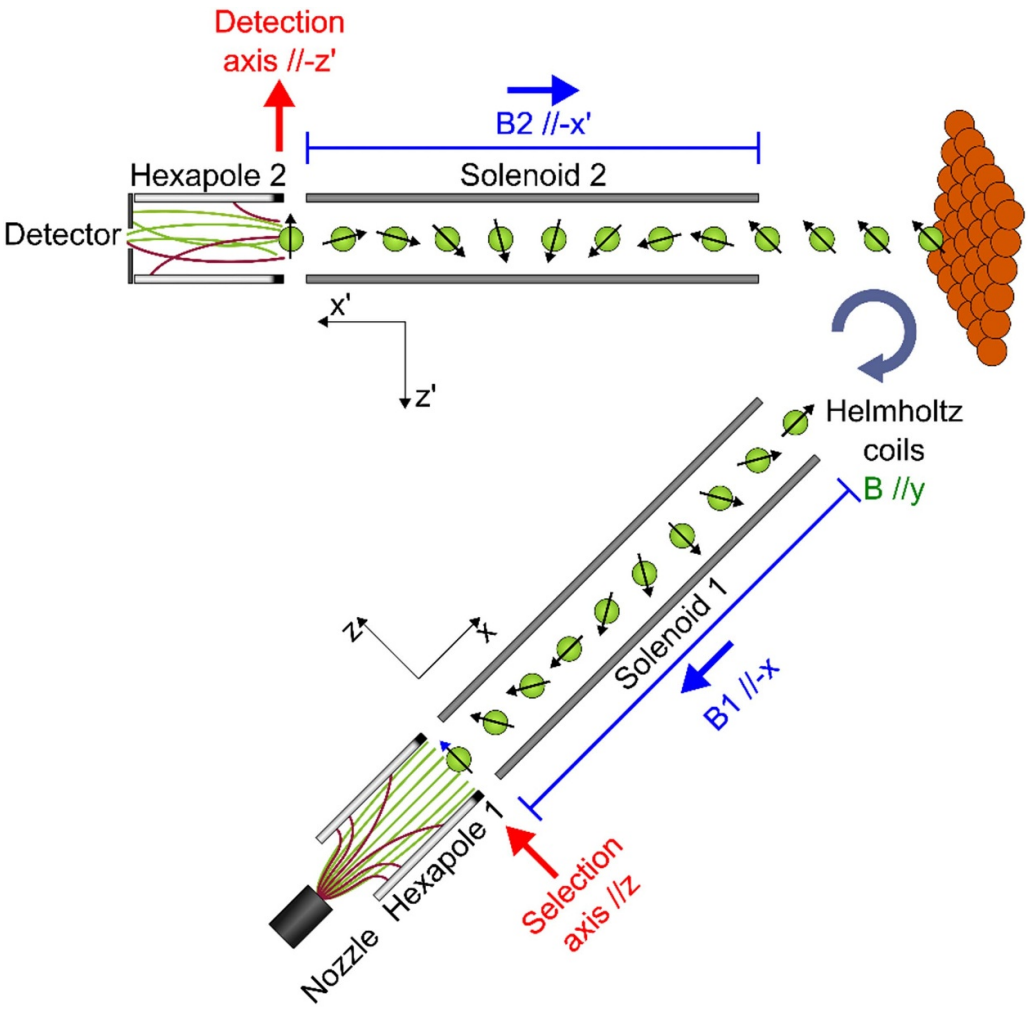

Figure 1. Schematic overview of the spin-echo apparatus showing the frames of reference for the first and second arms of the machine and the directions of the magnetic fields. The y and y' axes are directed into the plane of the page to maintain a right-handed co-ordinate system.

solenoids to stabilise before the measurement of the signal at a given field value.

3. Theoretical methods

To simulate the experiment, we need to calculate how the different m_I states are affected by the different magnetic fields that are present throughout the apparatus. For this we used a semi-classical model [10–13] where we propagate the spins through the different magnetic components of the beam path. Initially, the two m_I states are equally populated in the molecular beam expansion before the first hexapole. Semi-classical trajectory calculations are used to determine the probability that each m_I state is transmitted through the first hexapole [14, 19]. In the case of ^{3}He, these can be taken as 1 for the $m_I = {}^1/_2$ state and 0 for the $m_I = -{}^1/_2$ state, but if a more complex system is being studied these need to be determined for each magnetic state [11, 13].

The wavefunction for the $m_I = {}^1/_2$ state is then propagated through either an ideal magnetic field profile or the measured three-dimensional magnetic field profile of the first arm of the machine. In an ideal machine, this profile would correspond to a dipolar field along the z direction and a solenoid field along $\pm x$ direction for $\mp B_1$. The measured profile begins where the dipole field along the z direction is still sufficiently strong that the state is initially a pure state, and includes the rest of the dipole along the z direction as well as the measured solenoid profile along $-x$. However, there are also other small residual fields which can give rise to additional features in the measurements, and which must be included in the propagation to accurately reproduce the experimental data as we will demonstrate below. The spins are propagated through the magnetic field profiles using the Hamiltonian which is given by

$$H(B') = \frac{\hbar^2 k^2}{2m} - \gamma \boldsymbol{I} \cdot \boldsymbol{B'} \tag{1}$$

where the first term is the atoms kinetic energy which is related to its wavevector, k, and its mass, m, and the second term accounts for the interaction of the nuclear spins with the magnetic fields throughout the apparatus which depends on the gyromagnetic ratio, γ, the nuclear spin, $\boldsymbol{I}$ and the magnetic field $\boldsymbol{B'}$. This has the effect of Rabi oscillating the populations between the $m_I = -{}^1/_2$ and $m_I = {}^1/_2$ state as the atoms travel through the first solenoid, with the amplitudes and phases of

the two states at the end of the solenoid being dependent on the magnetic field strength. While strictly speaking both terms of the Hamiltonian need to be solved quantum mechanically, we will use a semi-classical description, where the centre of mass motion is treated classically and only the spin degrees of freedom are solved quantum mechanically. This type of approach has been compared to the fully quantum models for the case of elastic scattering of H_2, and has been shown to work very well, as long as the magnetic fields are not very strong (>10^4 gauss) [20].

We then simulate the scattering of the ^{3}He atoms from the Cu(111) surface as a simple purely-elastic reflection. As this is a non-magnetic surface, the nuclear spin states are not expected to be changed by the atom-surface interaction, i.e. all that needs to be included in the simulation is a rotation of the wavefunction which describes the states at the end of the first arm of the apparatus from the z quantisation axis to the z' quantisation axis which is used when propagating the wavefunction down the second arm of the machine. The propagation through the second arm is done in the same way as the first, i.e. using the Hamiltonian given in equation (1) to propagate the wavefunction through either an ideal magnetic field profile consisting of only the solenoid in the $\pm x'$ direction for $\mp B_2$ and dipole in the $-z'$ direction, or the measured magnetic field profile up to a point where the dipole field is sufficiently strong in the $-z'$ direction that the states no longer mix in the magnetic field. The transmission probabilities of the $m_I = -1/2$ and $m_I = 1/2$ states being transmitted through the second hexapole are again taken to be 0 and 1 respectively, where m_I is the projection of the nuclear spin on the direction of the dipole (along $-z'$). The signal is then calculated as the overlap integral of the wavefunction at the end of the propagation and summed (with appropriate weights) over the velocity distribution of the ^{3}He beam used in the experiments.

4. Results and discussion

4.1. The origin of the different spin-echoes

The top panel of figure 2 presents a two-dimensional simulated signal calculated for a simplified instrument, as is often assumed when analysing spin-echo experiments, for the specular scattering of ^{3}He from a surface. This means a linear instrument with an ideal magnetic beam profile. It shows one strong spin-echo condition at $B_1 = -B_2$, i.e. scanning the magnitude of the magnetic field along the $B_1 = -B_2$ diagonal line produces a constant signal, as depicted by the blue line in the bottom panel of the figure. As the scattering process considered was elastic, then the phase evolution is reversed for all the different velocities in the beam regardless of the value of $B_1 = -B_2$ and a constant signal along the condition is what we expect. Scanning perpendicularly to this constant intensity line, i.e. scanning the magnitude of the magnetic field along $B_1 = B_2$ produces an oscillating signal, often referred to as a spin-echo oscillation signal, as shown by the black line in the bottom panel of the figure, which has been normalised with respect to the mean of the signal. The oscillation frequency is dictated by the gyromagnetic ratio and the mean velocity

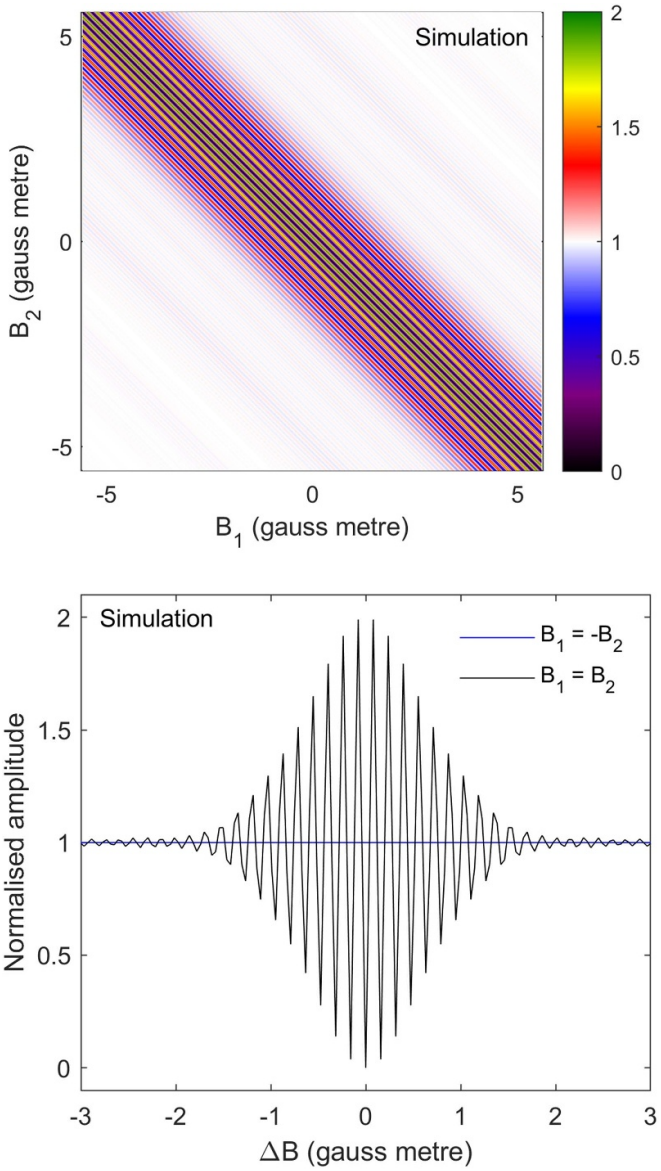

Figure 2. Top: two-dimensional plot of the signal intensity normalised with respect to the mean simulated for an ideal ^{3}He elastic scattering experiment. Bottom: one dimensional slices of the $B_1 = -B_2$ (blue) and $B_1 = B_2$ diagonals (black).

of the beam, and the envelope which peaks at the spin-echo condition is related to the energy/velocity distribution in the beam [6]. The x-axis in the bottom panel is the magnitude of the magnetic field integral $\Delta B \equiv \sqrt{{B_1}^2 + {B_2}^2}$, with negative/positive values corresponding to the sign of B_2.

For comparison with the idealised case, figure 3 presents a two dimensional plot of the signal, produced by performing B_1 scans measured at consecutive values of B_2 for the specular scattering of ^{3}He from a Cu(111) surface. It is immediately apparent that the measured intensity and the simulated intensity are significantly different, with there being a second diagonal feature as well as a horizontal and weaker vertical feature in the experimental data. There are therefore multiple spin-echoes even in the case of the elastic scattering of ^{3}He from a surface which have to be correctly accounted for when

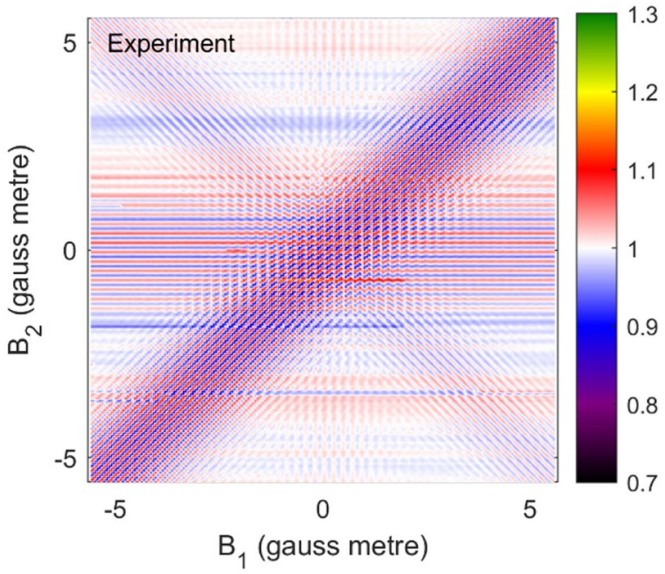

Figure 3. Two-dimensional plot of the signal intensity normalised with respect to the mean of ^{3}He scattering elastically from a Cu(111) surface measured at a surface temperature of 300 K.

using the technique to study phonons or adsorbate motion on the surface.

The idealised spin-echo signal presented in figure 2 was simulated for a linear machine. In reality, any scattering instruments will have a total scattering angle smaller than 180°, and the majority of the HSE studies have been performed using a scattering angle between the two arms of approximately 45°. A non-linear geometry has been previously [9] shown to give rise to a second diagonal echo at $B_1 = B_2$. The relative intensities of the two echoes depend on the angle between the two arms of the scattering apparatus, and the echo at $B_1 = B_2$ becomes the dominant echo condition for acute scattering angles [9]. The top panel of figure 4, which presents the results of a two-dimensional simulation for a total scattering angle of 46.2° (corresponding to that of the Swansea apparatus) illustrates this. One-dimensional scans for the $B_1 = -B_2$ (blue) and $B_1 = B_2$ (black) diagonals are shown in the bottom panel of the figure. These both produce signals which oscillate centred at $\Delta B = 0$ as opposed to the anticipated constant signal, oscillations which are the result of the intersection of the two diagonal echoes with each other. If the simplified picture of spin-echo measurements presented in figure 1 is used to interpret these results, i.e. the signal does not oscillate when ^{3}He is scattered elastically from the surface, then these oscillations could be incorrectly attributed to an inelastic scattering process when they are in fact simply due to the geometry of the machine.

Further complications arise due to the non-ideality of the magnetic field profile, as shown by the simulated data in figure 5 which has been calculated using the real magnetic field profile measured in the Swansea apparatus as opposed to an idealised model which only includes the (z) dipole and ($-x$) solenoid fields in the first arm, and the ($-z'$) dipole and ($-x'$) solenoid fields in the second arm. Using this realistic profile introduces both the stronger horizontal and weaker vertical

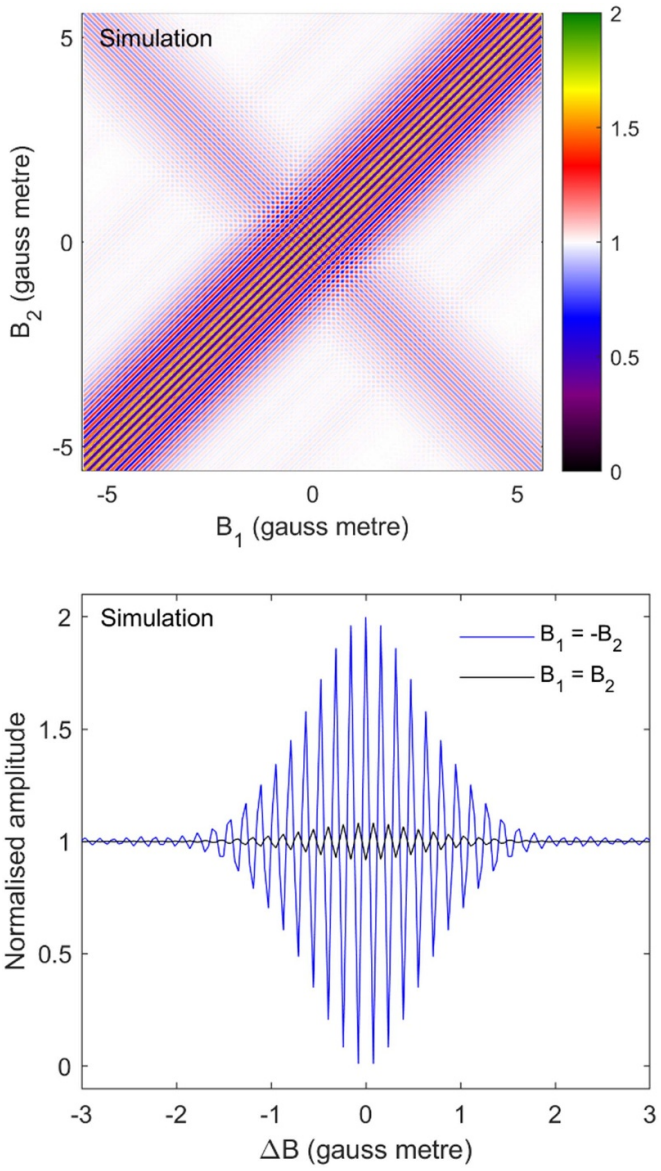

Figure 4. Top: two-dimensional plot of the signal intensity normalised with respect to the mean simulated for a ^{3}He elastic scattering experiment where the geometry of the machine is included but an ideal magnetic field profile is used. Bottom: one-dimensional slices of the $B_1 = -B_2$ (blue) and $B_1 = B_2$ diagonals (black).

echo into the simulated signal, as well as reproducing the two diagonal echoes discussed earlier. The horizontal echo, which resembles a plane wave starting at $B_2 = 0$ that is present at all B_1 values, has an intensity which oscillates and decays as a function of B_2 only. This echo, which has not been observed or predicted theoretically previously, is due to the presence of a small magnetic field along the x (propagation) direction at the end of the weak dipole of the first arm of the machine, which adiabatically rotates the spins from the z (first weak dipole) direction, to lie in the xz plane (see figure 1). It is also possible for this transition to have some non-adiabatic character, which causes the spin to precess around the direction of the magnetic field. This results in the spin also having a component along the y-axis as well as changing the x component. After

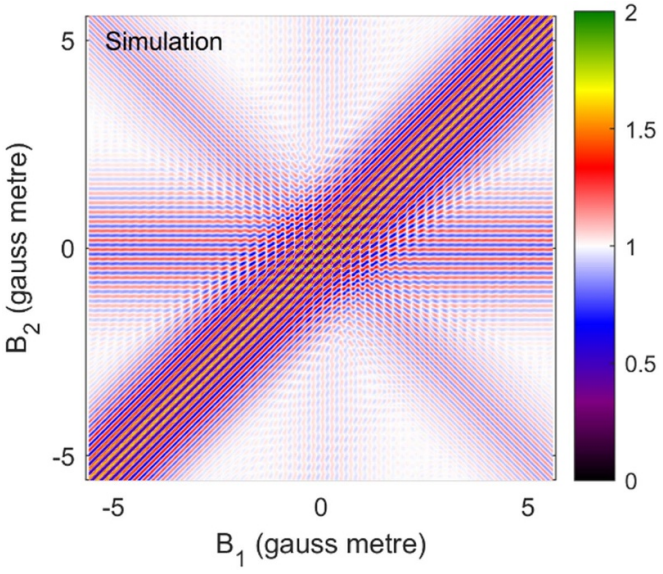

Figure 5. Two-dimensional plot of the signal intensity normalised with respect to the mean simulated for a ^{3}He elastic scattering experiment for a realistic machine. The much weaker X' echo is difficult to see and can be identified by the subtle white (low intensity) vertical stripes near the origin.

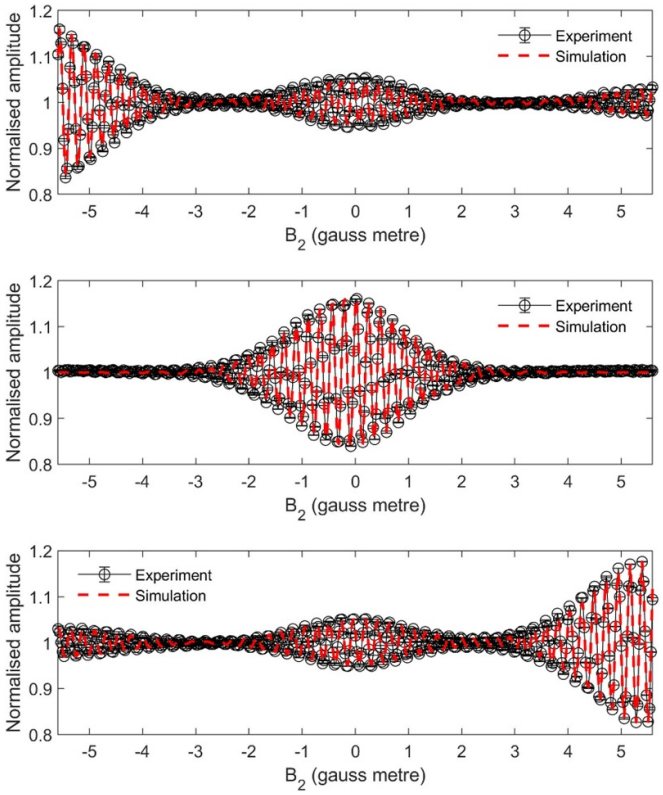

Figure 6. Top: a comparison of measured B_2 scans (black line and points) and simulated signals (red line) for $B_1 = -5.6$ gauss metre, where the signals have been normalised with respect to the mean. Middle: a comparison of measured B_2 scans (black line and points) and simulated signals (red line) for $B_1 = 0$ gauss metre, where the signals have been normalised with respect to the mean. Bottom: a comparison of measured B_2 scans (black line and points) and simulated signals (red line) for $B_1 = 5.6$ gauss metre, where the signals have been normalised with respect to the mean. While for $B_1 = 0$ (the middle panel) the contribution from all three echoes overlaps, they can be distinguished quite clearly in the presence of a large enough B_1 value (top and bottom panels).

the dipole, the x component of the spin remains unchanged as the atoms travel through the first solenoid as the magnetic field is either parallel or anti-parallel to the x direction, regardless of the particle velocity. This x component of the spin in the first arm of the machine can be separated into components which are parallel and perpendicular to $-x'$ in the second arm of the machine, which is the direction of B_2. Consequently, there is a spin component which is common to all velocities before the particles enter the second arm of the instrument. This component then precesses within the second magnetic field, leading to the observed oscillation pattern. The maximum of this additional echo lies along the horizontal $B_2 = 0$ line, and it oscillates and decays as B_2 is either increased or decreased, due to the spread in the velocities of the beam particles. We will refer to this phenomenon as the X echo, as it originates from the magnetic field of the weak dipole having a (typically small, but non-zero) x component.

The vertical echo arises from a similar phenomenon due to the non-ideality of the weak-dipole field in the second arm of the apparatus. The presence of a small field directed along the x' direction means that the final quantisation axis is not perpendicular to the x' direction along which B_2 is directed, which results in spins which are oriented along x' and $-x'$ being detected with slightly different probabilities. As the population of these states can be changed by scanning B_1, but are unaffected by the value of B_2, this produces an echo centred around $B_1 = 0$ gauss metre which is independent of B_2. We will refer to this echo as the X' echo, as it arises from the magnetic field of the second weak dipole having a small component along the x' direction.

The measured intensity (black) obtained when scanning B_2 at values of $B_1 = -5.6$ gauss metre (top) 0 gauss metre (middle) and 5.6 gauss metre (bottom) are compared to simulated signals (red) in figure 6. These three measurements contain oscillations arising from the parallel, anti-parallel and X echoes. As shown in the figure, the agreement between the experimental data and the simulations is excellent. This demonstrates that the simulations correctly capture the relative intensities, frequencies and phases of the different echoes that we observe in the measurements. They therefore provide a useful diagnostic tool, in the sense that if oscillations are seen in future experiments which are reproduced in the simulations this indicates that they are either related to the geometry of the experiment (in the case of the parallel and anti-parallel echoes) or the non-ideality of the magnetic field profile in the machine (in the case of the X and X' echoes).

The intensity of each of the echoes can be changed with the addition of a magnetic field directed along the y-axis at the end of the first solenoid [9], which is generated using a set of Helmholtz coils as shown schematically in figure 1. Originally, a Helmholtz coil producing a magnetic field along the y-axis, was introduced as part of a HSE apparatus to increase the polarisation and compensate for the polarisation loss due to

the finite scattering angle [5, 18]. Further, more detailed analysis showed that such a field can change the relative intensities of the two diagonal echoes [9]. Below we show that this y field can change the intensities of all the echoes mentioned above and depending on the current passed through the Helmholtz coils, the spurious spin-echo signals which exist in a realistic setup can be minimised.

The effect of scanning this additional y field on the intensity of the parallel (blue), anti-parallel (red), X (black) and X' (green) echo is shown in the top panel of figure 7. For the parallel echo measurement, $B_1 = B_2 \approx 110$ gauss metre, the anti-parallel measurement $B_1 = -B_2 \approx 110$ gauss metre, for the X echo measurement, $B_1 \approx 110$ gauss metre and $B_2 \approx 0$ gauss metre and for the X' echo measurement, $B_1 \approx 0$ gauss metre and $B_2 \approx 110$ gauss metre. The maximum intensity of the parallel echo is achieved when the intensity of the anti-parallel echo is minimised, and vice versa. For these two echoes, the maximum in the intensity corresponds to the maximum oscillation amplitude whereas the minimum corresponds to there being no echo. This is not true for the X and X' echoes, where the maximum and minimum in the intensity plot correspond to the maximum amplitude oscillation but the two oscillations are out of phase with each other, as shown by the blue (minimum intensity) and black (maximum intensity) lines in the top panel of figure 8 for the X echo, and the green (minimum intensity) and black (maximum intensity) lines in the bottom panel for the X' echo. The intensity of the X echo is minimised when the normalised signal shown in figure 8 has a value of 1. In principle, the parallel echo intensity is maximised when the anti-parallel, X and X' echoes intensity are minimised, but here this is not quite the case, most likely due to the Helmholtz field having a small but non-zero component along the x and/or z directions. However, this still demonstrates that it is possible to suppress the influence of the other echoes on a measurement which maximises the intensity of the anti-parallel echo by using a small y field. The bottom panel of figure 7 presents the two-dimensional intensity obtained from such a measurement, where a Helmholtz field of 0.03 gauss metre was used to maximise the parallel echo intensity and minimise the amplitude of the others. Whilst this has reduced the intensity of the anti-parallel, X and X' echoes, traces of each are still visible in the measured intensity as complete cancellation would only be achieved for a monochromatic beam as the phase accumulated due to the Helmholtz coils is velocity dependent.

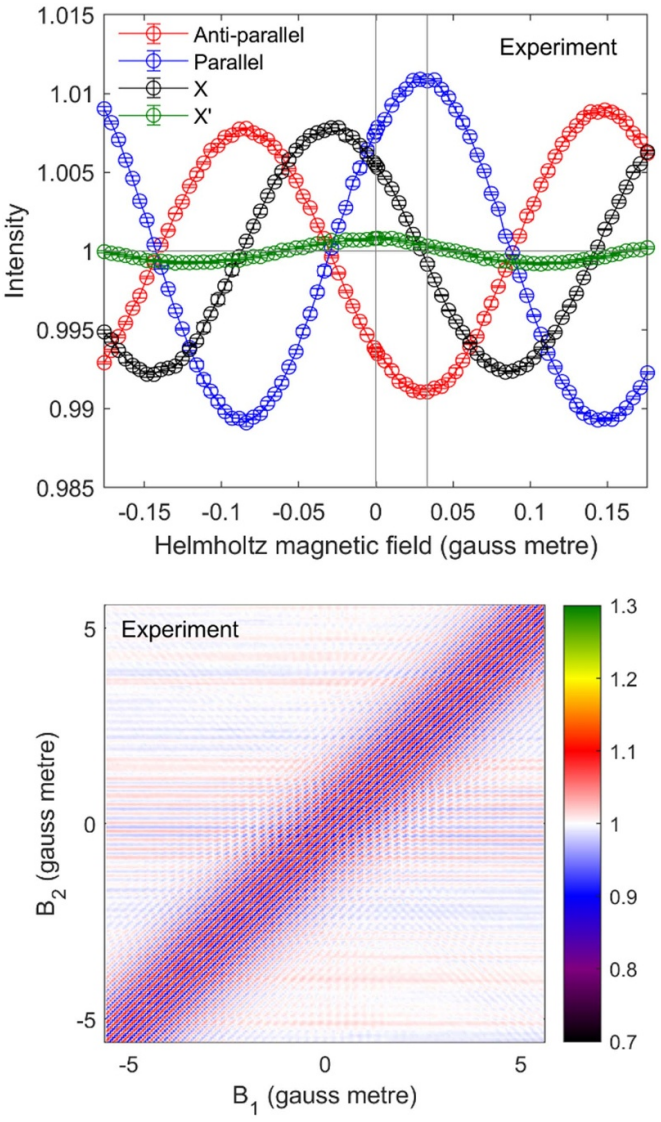

Figure 7. Top: the intensity of the anti-parallel echo (red), parallel echo (blue), X echo (black) and X' echo (green) normalised so that the mid-point of the oscillation is 1 as a function of the magnetic field applied along the y direction at the end of the first solenoid. In each case, the values of B_1 and B_2 were kept at a constant value which corresponded to the maximum of the echo oscillation. The vertical lines show the magnetic field values which were used for the 2d scans shown in figure 3 and the bottom panel of this figure. Bottom: two-dimensional plot of the signal intensity normalised with respect to the mean of ^{3}He scattering elastically from a Cu(111) surface measured at a surface temperature of 300 K with a y field of approximately 0.03 gauss metre to minimise the intensity of the anti-parallel echo.

4.2. The effect of multiple echoes when analysing two-dimensional spin-echo measurements

As mentioned earlier, the different echoes in the signal arise when particles with different velocities in the beam have a common spin phase at a given magnetic field value. A simple framework for understanding the spin echo signals generated by elastic and inelastic scattering, and how to measure them in an optimal way is the tilted projection picture [5]. Below we give a brief description of this picture, more detailed explanations can be found in previous publications [2, 5–7], before we examine how the multiple echoes discussed above modify these results.

Classically, the phase that the magnetic moment of ^{3}He atoms acquire in a magnetic field with a strength B' is given by $B'\gamma t$, where γ is the gyromagnetic ratio and t is the time the atom is in the magnetic field. Rewriting the time as the length of the field, L, divided by the velocity of the atoms, v, and defining the magnetic field integral, B as $B'L$ allows the total phase to be rewritten as $\frac{B\gamma}{v}$. Expressing the velocity in terms of the de-Broglie wavelength, λ gives $\frac{mB\gamma\lambda}{h}$, where m is the mass and h is Planck's constant. It follows that when the dipole

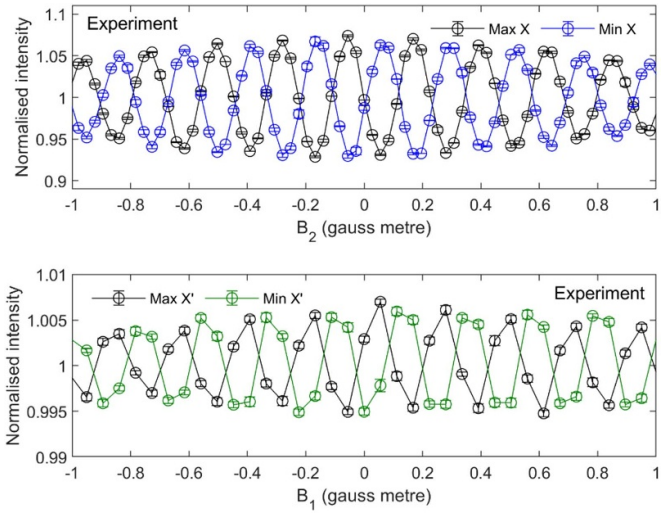

Figure 8. Top: B_2 scan where $B_1 \approx 110$ gauss metre for different values of magnetic field directed along the y-axis which show the changing phase of the X echo, the two traces correspond to y field values which maximise and minimise the amplitude of that echo. Bottom: a similar plot, this time showing B_1 scans where $B_2 \approx 110$ gauss metre for different values of magnetic field directed along the y-axis which show the changing phase of the X' echo. In both panels the signal intensity has been normalised with respect to the mean.

fields which define the quantisation axis of both the polariser and analyser hexapoles are aligned along the same direction, the signal for a beam of atoms with a single velocity travelling through one magnetic field, and after subtracting a constant term, is proportional to $\cos\left(\frac{mB\gamma\lambda}{h}\right) = \cos(2\pi\kappa\lambda)$ where $\kappa = \frac{mB\gamma}{2\pi h}$.

When there is a spread of velocities which contribute to the signal, and when the atoms travel through two magnetic fields, the signal is given by $S_{\mathrm{r}}(\kappa_1,\kappa_2) \propto \int_{-\infty}^{\infty}\int_{-\infty}^{\infty}\rho\ (\lambda_1,\lambda_2)$ $\cos\left(2\pi\kappa_1\lambda_1 + 2\pi\kappa_2\lambda_2\right) d\lambda_1 d\lambda_2 + C$, where $\rho(\lambda_1,\lambda_2)$ is the probability density that the ^{3}He atoms have a wavelength λ_1 before scattering and λ_2 after scattering, elastic scattering is characterised by $\lambda_1 = \lambda_2$ and inelastic scattering by $\lambda_1 \neq \lambda_2$ and $n = 1,2$ denote the first and second arm of the machine respectively. C is a constant term related to the unpolarised intensity, which can be subtracted from the measurement. If an additional 90° rotation of the spins is performed after exiting the polariser an additional signal S_{im} can be measured which is identical to S_{r} but has a sine instead of a cosine in the integral. Finally, a complex signal can be defined as $S(\kappa_1,\kappa_2) = S_{\mathrm{r}} + \sqrt{-1}S_{\mathrm{im}}$ and performing a two-dimensional Fourier transform on $S(\kappa_1,\kappa_2)$ allows us to reconstruct the wavelength intensity matrices $\rho(\lambda_1,\lambda_2)$ from the measurements. If only the real part of $S(\kappa_1,\kappa_2)$ is measured the Fourier transform yields a symmetrised form of $\rho(\lambda_1,\lambda_2)$ which contains mirror images of the true wavelength intensity matrix. As we will show below, other features will also appear after Fourier transforming the signal, to distinguish the actual intensity matrix $\rho(\lambda_1,\lambda_2)$ characterising the physical scattering event from that obtained by Fourier transforming the measurement,

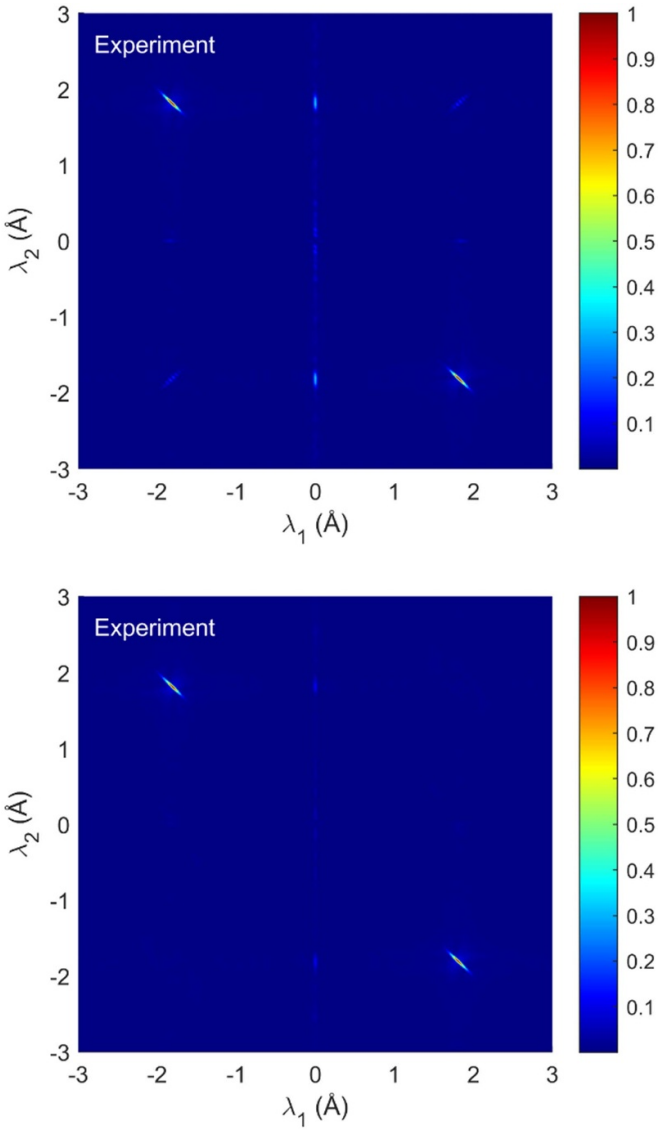

Figure 9. Top: two-dimensional wavelength intensity plot normalised with respect to the maximum intensity obtained by taking the Fourier transform of the experimental data presented in figure 3 without the additional y field. Bottom: normalised two-dimensional wavelength intensity plot obtained by taking the Fourier transform of the experimental data presented in figure 7 where a 0.03 gauss metre y field is used to minimise the anti-parallel echo.

we will denote the latter reconstructed wavelength matrices $\rho'(\lambda_1,\lambda_2)$.

Reconstructed wavelength intensity matrices are presented in the top and bottom panels of figure 9 for the data presented in figures 3 and 7 respectively. They have been normalised to the maximum intensity in each case. In the top panel, which corresponds to the measurement presented in figure 3 performed without using the Helmholtz coils to generate a y field, the intensity at $\lambda_1 = \lambda_2$ corresponds to the antiparallel echo, and the intensity at $\lambda_1 = -\lambda_2$ corresponds to the parallel echo. The relative intensities depend on the angle between the two arms of the machine in the same way as the corresponding echoes [9]. The intensity at $\lambda_1 = 0$ Å and $\lambda_2 \approx \pm 1.8$ Å

is due to the X echo, and the weak intensity at $\lambda_1 \approx \pm 1.8$ Å and $\lambda_2 = 0$ Å is due to the X'-echo. The intensity at $\lambda_1 = 0$ Å and $|\lambda_2| < 1$ Å is an artifact due to the drift in the baseline of the measurement during the length of the two-dimensional scan. In the bottom panel, due to the additional applied y field, the intensity at $\lambda_1 = \lambda_2$ and that from the X' echo have been removed, leaving only the features at $\lambda_1 = -\lambda_2$ and from the X echo. The peak for each echo has a mirror image because only the real (cosine) component of the data was measured, with only the polarisation with respect to the z'-axis being recorded. These additional peaks can be removed by also measuring the polarisation with respect to the y'-axis and analysing the data as a complex signal [6]. Simulations have shown that this would remove the peaks with $\lambda_1 < 0$ Å and the $\lambda_1 = 0$ Å, $\lambda_2 < 0$ Å peak for the X echo, meaning only one peak would be seen in the wavelength intensity matrix for each of the four echoes.

4.3. The effect of multiple echoes when analysing one-dimensional spin-echo measurements

Whilst figure 9 illustrates that the additional echo conditions give rise to various spurious features in the reconstructed wavelength intensity, they are positioned at wavelength values which make no physical sense and would not be erroneously interpreted as being due to inelastic scattering. However, the two-dimensional measurements which are required to reconstruct a wavelength matrix require extremely long acquisition times and are generally not feasible for surfaces which have any significant reactivity to contamination. This long acquisition time is related to the simultaneous need to scan using small ΔB steps, to avoid signal aliasing, and up to large values of B_1 and B_2, to improve the resolution of the wavelength intensity matrix obtained from Fourier transforming the measurement. To the best of our knowledge, reconstruction of a wavelength intensity matrix for inelastic scattering has only been performed once [7]. To circumvent the long acquisition time, the overwhelming majority of spin-echo measurements are one-dimensional scans in the B_1, B_2 plane including, for example, a wide range of surface diffusion experiments (some of which were reviewed by Jardine *et al* [2]), measurements of inter-adsorbate interactions [21, 22], selective adsorption of helium atoms [23], dispersion relations, anharmonicity, and lifetimes of surface phonons [5, 6, 24], dispersion relations and lifetimes of adsorbate vibrations [25–27], and the dynamics of partial dislocations [28].

A general type of one-dimensional spin echo experiment is sometimes termed a tilted projection measurement [5, 6], which corresponds to one-dimensional scans of the magnitude of the two magnetic fields along $B_1 = \alpha B_2$, where α is some proportionality constant chosen depending on the information that is being extracted from the experimental data. In a typical spin-echo experiment which focuses on quasi-elastic scattering, magnetic field scans are performed by scanning the field while maintaining the condition $B_1 = B_2$ or $B_1 = -B_2$. Simple spin-echo theories, used so far, predict the signal in such a measurement to be constant when measuring pure elastic scattering, decay as a function of the magnitude of B

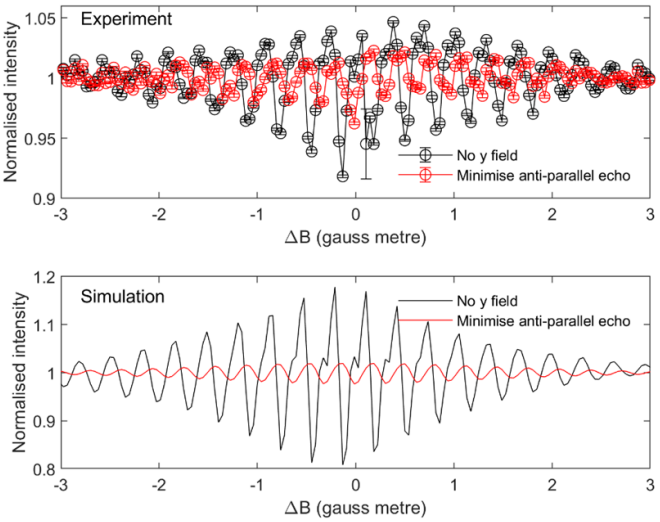

Figure 10. Top: magnetic field scans where the fields in the solenoid are maintained at the condition $B_1 = B_2$ when there is no additional y field (black lines) and with a y field of approximately 0.03 gauss metre to minimise the intensity of the anti-parallel echo (red lines), normalised with respect to the mean. Bottom: simulations of the measurements presented in the top panel, normalised with respect to the mean.

in the presence of quasi-elastic scattering due to the random motion of the surface particles (surface diffusion) and oscillate in the presence of inelastic scattering (e.g. scattering from surface phonons). When measuring inelastic scattering, a much improved resolution can be obtained by using different values for the proportionality constant α, values chosen to make the measurement scan perpendicular to direction of the inelastic feature in λ_1, λ_2 space, and reduce the broadening related to the finite beam velocity distribution [5, 6].

Measurements for the simpler and most widely used condition $\alpha = 1$ are presented in the top panel of figure 10, where the black line corresponds to the case where there is no additional y field (corresponding to the two-dimensional scan in figure 3), and the red line where the additional y field cancels the intensity of the anti-parallel echo (the two-dimensional scan in the bottom panel of figure 7). The measurements are performed at specular scattering conditions and should be completely dominated by pure elastic scattering. Nevertheless, in each case, oscillations are seen in the spin-echo measurements, which could be erroneously interpreted as being due to inelastic scattering processes occurring on the surface. However, as shown by the simulations presented in the bottom panel of the figure, these oscillations are again correctly reproduced in the simulated data when the angle of the machine and non-ideal nature of the magnetic field profile are incorporated into the calculation. It should be noted that the amplitudes are different in the case of the measured and simulated signals due to unknown polarisation losses which occur due to the transitions between the different magnetic fields throughout the apparatus which reduces the amplitude of the measured oscillations.

The Fourier transform of the data in the tilted projection measurement presented in figure 10 corresponds to the

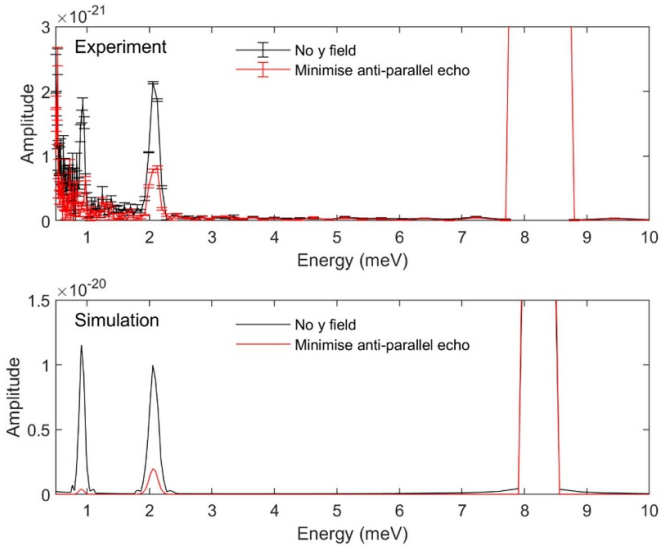

Figure 11. Top: the apparent energies of the scattered ^{3}He atoms corresponding to the spin-echo measurements presented in the top panel of figure 10. Bottom: the apparent energies of the scattered ^{3}He atoms corresponding to the simulations presented in the bottom panel of figure 10.

projection of the peaks in the two-dimensional wavelength intensity matrix onto the line that is being measured, i.e. the $\lambda_1 = \lambda_2$ line [5, 6]. This means that the projection of all the echoes shown in figure 9 will contribute to the spectrum, even the artificial mirror peaks, and it will be less apparent in the one-dimensional measurement that these peaks are not due to inelastic scattering. If not properly accounted for, these can be inadvertently assigned to be signatures of inelastic scattering, as demonstrated below.

The results of analysing the oscillations presented in figure 10 in terms of apparent scattered energy are shown in figure 11, where the lines in the figure correspond to those presented in figure 10 and the top panel corresponds to the measured signal and the bottom the simulated signal. In each case, an elastic scattering peak is observed at 8.6 meV which corresponds to the incident energy of the atomic beam of ^{3}He. Where the additional y field is set to zero, two apparently inelastic scattering features are observed, one at an energy of 2.1 meV and one at an energy of 0.9 meV. When the additional y field is used to remove the anti-parallel echo from the data and increase the intensity of the parallel echo, which is typically done to maximise the signal intensity in spin-echo measurements, an apparently inelastic feature is still present in the spectrum. However, the fact that this is seen in the spectrum for the simulated data which was calculated for pure elastic scattering verifies that this feature is not a signature of inelastic scattering in this case and arises simply due to the presence of the X echo. It also further illustrates the importance of simulations that include both the geometry of the machine and the non-ideality of the magnetic field profile of the apparatus in accurately interpreting spin-echo measurements.

5. Summary

In the current work we have demonstrated that multiple echoes exist even in the simplest case of a spin $^1/_2$ particle scattering elastically from a surface. The first of these corresponds to the condition $B_1 = -B_2$, where the phase that the atoms accumulate through precession in the first magnetic field is reversed due to their equal and opposite precession in the second. A second echo arises due to the geometry of the machine at $B_1 = B_2$, and another two exist due to the non-ideal magnetic field that exists in a real spin-echo apparatus, one of which is only a function of B_1, the other a function of only B_2. Whilst the influence of these additional echoes can be minimised in experiments used to probe ultra-fast surface dynamics by the addition of a small magnetic field in the y direction, this does not completely remove the oscillations due to the finite velocity spread of the atomic beam and small magnetic field components along the x and z directions.

Spin-echo experiments are typically analysed using a simplistic model of the phenomenon which considers the presence of only a single spin-echo in a scattering experiment. By not including the additional echoes, it is possible that these will be misinterpreted as signatures of inelastic scattering, with the likelihood of this being higher when 1-dimensional measurements are performed. However, we have also demonstrated that by propagating the spins through the measured magnetic field profile of the apparatus it is possible to accurately reproduce all the different spin-echoes with the correct frequency and relative intensity. It is therefore essential to use this complete picture when analysing spin-echo measurements to determine if the observed oscillations are due to an inelastic scattering event or simply due to the non-ideality of the experimental apparatus.

Data availability statement

The data that support the findings of this study are available upon reasonable request from the authors.

Acknowledgments

This work was funded by a European Commission, Horizon 2020 Framework Programme, H2020 Excellent Science, H2020 European Research Council Consolidator Grant No. 772228, and a Research Councils UK, Engineering and Physical Sciences Research Council New Horizons Grant Number EP/V048589/1.

ORCID iDs

Helen Chadwick https://orcid.org/0000-0003-4119-6903
Joshua T Cantin https://orcid.org/0000-0001-7088-8699

References

[1] Mezei F, Pappas C and Gutberlet T 2002 *Neutron Spin Echo Spectroscopy: Basics, Trends and Applications* vol 601 (Berlin: Springer)

[2] Jardine A P, Alexandrowicz G, Hedgeland H, Allison W and Ellis J 2009 Studying the microscopic nature of diffusion with helium-3 spin-echo *Phys. Chem. Chem. Phys.* **11** 3355–74

[3] Mezei F 1980 The principles of neutron spin echo *Neutron Spin Echo* (Berlin: Springer) pp 1–26

[4] Gähler R, Golub R, Habicht K, Keller T and Felber J 1996 Space-time description of neutron spin echo spectrometry *Physica* B **229** 1–17

[5] Alexandrowicz G 2005 Helium spin echo spectroscopy: measuring the dynamics of atoms, molecules and surfaces *PhD Thesis* University of Cambridge

[6] Alexandrowicz G and Jardine A P 2007 Helium spin-echo spectroscopy: studying surface dynamics with ultra-high-energy resolution *J. Phys.: Condens. Matter* **19** 305001

[7] Kole P R, Jardine A P, Hedgeland H and Alexandrowicz G 2010 Measuring surface phonons with a ^{3}He spin echo spectrometer: a two-dimensional approach *J. Phys.: Condens. Matter* **22** 304018

[8] Levitt M H 2013 *Spin Dynamics: Basics of Nuclear Magnetic Resonance* (New York: Wiley)

[9] Litvin I, Alkoby Y, Godsi O, Alexandrowicz G and Maniv T 2019 Parallel and anti-parallel echoes in beam spin echo experiments *Results Phys.* **12** 381–91

[10] Godsi O, Corem G, Alkoby Y, Cantin J T, Krems R V, Somers M F, Meyer J, Kroes G J, Maniv T and Alexandrowicz G 2017 A general method for controlling and resolving rotational orientation of molecules in molecule-surface collisions *Nat. Commun.* **8** 15357

[11] Alkoby Y, Chadwick H, Godsi O, Labiad H, Bergin M, Cantin J T, Litvin I, Maniv T and Alexandrowicz G 2020 Setting benchmarks for modelling gas–surface interactions using coherent control of rotational orientation states *Nat. Commun.* **11** 3110

[12] Chadwick H, Alkoby Y, Cantin J T, Lindebaum D, Godsi O, Maniv T and Alexandrowicz G 2021 Molecular spin echoes; multiple magnetic coherences in molecule surface scattering experiments *Phys. Chem. Chem. Phys.* **23** 7673–81

[13] Chadwick H, Somers M F, Stewart A C, Alkoby Y, Carter T J D, Butkovicova D and Alexandrowicz G 2022 Stopping molecular rotation using coherent ultra-low-energy magnetic manipulations *Nat. Commun.* **13** 2287

[14] Jardine A P, Fouquet P, Ellis J and Allison W 2001 Hexapole magnet system for thermal energy ^{3}He atom manipulation *Rev. Sci. Instrum.* **72** 3834–41

[15] Utz M, Levitt M H, Cooper N and Ulbricht H 2015 Visualisation of quantum evolution in the Stern–Gerlach and Rabi experiments *Phys. Chem. Chem. Phys.* **17** 3867–72

[16] Dworski S, Alexandrowicz G, Fouquet P, Jardine A P, Allison W and Ellis J 2004 Low aberration permanent hexapole magnet for atom and molecular beam research *Rev. Sci. Instrum.* **75** 1963–70

[17] Bergin M, Ward D J, Lambrick S M, von Jeinsen N A, Holst B, Ellis J, Jardine A P and Allison W 2021 Low-energy electron ionization mass spectrometer for efficient detection of low mass species *Rev. Sci. Instrum.* **92** 73305

[18] Fouquet P, Jardine A P, Dworski S, Alexandrowicz G, Allison W and Ellis J 2005 Thermal energy ^{3}He spin-echo spectrometer for ultrahigh resolution surface dynamics measurements *Rev. Sci. Instrum.* **76** 53109

[19] Krüger C, Lisitsin-Baranovsky E, Ofer O, Turgeon P-A, Vermette J, Ayotte P and Alexandrowicz G 2018 A magnetically focused molecular beam source for deposition of spin-polarised molecular surface layers *J. Chem. Phys.* **149** 164201

[20] Cantin J T, Alexandrowicz G and Krems R V 2020 Transfer-matrix theory of surface spin-echo experiments with molecules *Phys. Rev.* A **101** 062703

[21] Alexandrowicz G, Kole P R, Lee E Y M, Hedgeland H, Ferrando R, Jardine A P, Allison W and Ellis J 2008 Observation of uncorrelated microscopic motion in a strongly interacting adsorbate system *J. Am. Chem. Soc.* **130** 6789–94

[22] Tamtögl A, Bahn E, Sacchi M, Zhu J, Ward D J, Jardine A P, Jenkins S J, Fouquet P, Ellis J and Allison W 2021 Motion of water monomers reveals a kinetic barrier to ice nucleation on graphene *Nat. Commun.* **12** 3120

[23] Jardine A P, Dworski S, Fouquet P, Alexandrowicz G, Riley D J, Lee G Y H, Ellis J and Allison W 2004 Ultrahigh-resolution spin-echo measurement of surface potential energy landscapes *Science* **304** 1790–3

[24] Tamtögl A, Campi D, Bremholm M, Hedegaard E M J, Iversen B B, Bianchi M, Hofmann P, Marzari N, Benedek G and Ellis J 2018 Nanoscale surface dynamics of Bi_2Te_3(111): observation of a prominent surface acoustic wave and the role of van der Waals interactions *Nanoscale* **10** 14627–36

[25] Jardine A P, Alexandrowicz G, Hedgeland H, Diehl R D, Allison W and Ellis J 2007 Vibration and diffusion of Cs atoms on Cu (001) *J. Phys.: Condens. Matter* **19** 305010

[26] Jardine A P, Hedgeland H, Ward D, Xiaoqing Y, Allison W, Ellis J and Alexandrowicz G 2008 Probing molecule–surface interactions through ultra-fast adsorbate dynamics: propane/Pt (111) *New J. Phys.* **10** 125026

[27] Lechner B A J, Hedgeland H, Jardine A P, Allison W, Hinch B J and Ellis J 2015 Vibrational lifetimes and friction in adsorbate motion determined from quasi-elastic scattering *Phys. Chem. Chem. Phys.* **17** 21819–23

[28] McIntosh E M, Kole P R, El-Batanouny M, Chisnall D M, Ellis J and Allison W 2013 Measurement of the phason dispersion of misfit dislocations on the Au (111) surface *Phys. Rev. Lett.* **110** 86103